Italian Journal of Engineering Geology and Environment
www.ijege.uniroma1.it

ASSESSMENT OF MT-INSAR PROCESSING TECHNIQUES FOR SLOW-MOVING LANDSLIDES MONITORING IN CUENCA (ECUADOR) THROUGH DOUBLE-BAND SAR SATELLITE

Mohammad Amin KHALILI[(*)], Luigi GUERRIERO[(*)], Silvio CODA[(*)], Chester SELLERS[(**)], Domenico CALCATERRA[(*)] & Diego DI MARTIRE[(*)]

[(*)]Federico II University of Naples - Department of Earth, Environmental and Resource Sciences - Monte Sant'Angelo Campus - Naples, Italy
[(**)]University of Azuay - IERSE - Cuenca, Ecuador
Corresponding author: mohammadamin.khalili@unina.it

EXTENDED ABSTRACT

Le frane sono tra i fenomeni naturali che hanno maggior impatto sulla popolazione al mondo. Diverse tecniche di telerilevamento sono state utilizzate per studiare questi fenomeni negli ultimi decenni, inclusi Global Navigation Satellite Systems (GNSS) e l'Interferometria Differenziale SAR (DInSAR).

L'area dove sono presenti le strutture dell'Università di Azuay (Cuenca - Ecuador) e le vicine infrastrutture di trasposto sono state interessate nel tempo da frane a cinematica lenta. Gli eventi gravitativi hanno impattato sia settori urbanizzati nella zona di coronamento dove sono stati registrati i maggiori effetti, e sia aree non urbanizzate nella zona di piede. Per investigare in modo completo l'estensione e la cinematica dell'area in frana è stato necessario utilizzare due distinti approcci, applicati ad immagini SAR satellitari, il primo PS-like ha consentito di investigare le zone maggiormente urbanizzate, il secondo, Distributed-like, per investigare le aree maggiormente coperta da vegetazione.

A tal fine, due serie di immagini SAR, acquisite in banda X (COSMO-SkyMed (CSK)) e C (Sentinel-1 (S1-A)), rispettivamente, sono state analizzate e confrontate per il monitoraggio delle deformazioni.

Le tecniche PS-like e Distributed-like sono state utilizzate per misurare i tassi di deformazione superficiale e le serie temporali di spostamento riferite ai periodi 2017-2019 (S1-A) e 2015-2018 (CSK). I risultati ottenuti mediante tali approcci sono stati integrati e georiferiti mediante l'utilizzo di una vicina stazione GNSS, installata in un'area non interessata da deformazioni.

Al fine di determinare gli intervalli più appropriati per la preparazione delle mappe dei tassi di deformazione media, è stato utilizzato un algoritmo di apprendimento automatico non supervisionato (K-Medians). Infine, è stato effettuato un confronto tra gli output ottenuti da questo studio e lo spostamento registrato in corrispondenza di due ulteriori stazioni GNSS situate nell'area interessata dalle deformazioni. I risultati ottenuti dal monitoraggio SAR a doppia banda ed il confronto tra le diverse tecniche di elaborazione delle immagini hanno consentito di analizzare in maniera efficace e completa la cinematica dei fenomeni dell'intera area di studio.

IJEGE, Special Issue 1 (2023): 81-88, DOI: 10.4408/IJEGE.2023-01.S-11
E-ISSN 2035-5688 | ISSN 1825-6635 /

ABSTRACT

Landslides are among the most intense geological disasters worldwide. Several remote sensing techniques have been used to study these phenomena over the last few decades, including Global Navigation Satellite Systems (GNSS) and Multi-Temporal Interferometric Synthetic Aperture Radars (MT-InSAR), in particular, Small Baseline Subset (SBAS) and Permanent Scatterer Interferometry (PSI). The University of Azuay and highway infrastructure (Cuenca - Ecuador) were affected by slow-moving landslides which in urban areas had more noticeable deformation effects due to their crowns. Furthermore, evidence indicates that the landslide toe was developed in a rural area. To study landslide boundary and deformation kinematics comprehensively, we need to observe two distinct scattering surfaces using SAR imagery (high coherence areas in the urban area and low coherence areas in the rural area). We can also observe different distributions in X- and C-bands due to the rural area covered by vegetation and trees at the toe of the landslide. Two sets of radar images were analyzed and compared for monitoring the aforementioned slow-moving landslide kinematics, including Sentinel1-A (S1-A) and COSMO-SkyMed (CSK). PSI and SBAS techniques have been used to measure the rate of surface deformation and displacement time series at CSK over the period (2017-2019) and S1-A units over the period (2015-2018), respectively. Furthermore, a GNSS station in the stable area was used as a reference station to integrate the PSI and SBAS results over space. Then, an unsupervised machine learning algorithm (K-medians) was used to determine the most appropriate intervals for preparing mean deformation rate maps. Finally, a comparison was made between the outputs obtained from this study and displacement recorded at two additional GNSS stations located in the area affected by deformation. As a result, by comparing and monitoring double-band SAR satellites and different SAR image processing techniques, it became possible to analyze the whole landslide of our case study appropriately.

Keywords*: landslides, PSI, SBAS, COSMO-SkyMed mission, sentinel mission, Cuenca*

INTRODUCTION

Landslides represent one of the most frequent and impacting geological phenomena on a global scale. The extensive scientific literature on this topic attests to their worldwide distribution and the severe consequences they can have on the built environment and human life (Ajmera & Tiwari, 2021; Lu *et alii*, 2021). Technological progress is constantly producing new improvements for surveying and computational capabilities, providing more sophisticated tools to investigate this kind of natural process (Ghorbanzadeh *et alii*, 2022; Petrucci, 2022).

Therefore, developing remote sensing and earth-monitoring technologies can help to address global challenges such as disaster prevention, deformation monitoring (Coda *et alii*, 2019, Allocca *et alii*, 2021), and risk assessments. Various remote sensing techniques have been developed to study the deformation caused by landslides, including GNSS (Atanasova-Zlatareva & Nikolov, 2017) and MT-InSAR (Wasowski & Bovenga 2014, Del Soldato *et alii*, 2021; Foumelis *et alii*, 2016; Soltanieh & Macciotta, 2022). GNSS stations in stable areas are used for spatial coordination and adjustment, whereas GNSS stations affected by deformation are used for evaluating and comparing SAR image processing results. The MT-InSAR technique can provide millimeter-precision and high spatial resolution for determining the deformation rate map over a wide area (Miele *et alii*, 2021).

Several techniques have been developed since the inception of InSAR technology to improve precision. InSAR is a type of two SAR image processing technique (Gabriel *et alii*, 1989), while MT-InSAR is a multi-SAR image processing technique. The differential principle can be combined with time series analyses, such as a SBAS (Berardino *et alii,* 2002, Hooper, 2008) and PSI (Ferretti *et alii*, 2001). Each method (i.e., SBAS and PSI) has its benefits and drawbacks when retrieving spatiotemporal aspects of surface deformations over short and long periods of time. SBAS technique utilizes a series of interferograms characterized by small spatio-temporal baselines. This technique retrieves time-series cumulative deformation using the distributed scatterers (DS) (Lanari *et alii*, 2004), which are more available in rural areas. While in the PSI method, deformation is measured only over Permanent Scatterers (PS), which are prevalent and denser in urban environments (Guerriero *et alii*, 2019). In this area, the presence of buildings operating as natural reflectors due to their backscattering capabilities allows images to remain coherent. Moreover, comparatively to PSI, the SBAS method uses DS pixels with shorter time coherence behavior. Thus, we can investigate and analyze displacements in urban areas by applying the PSI method. However, when landslides inventory maps and geological settings (Sellers *et alii*, 2021) indicate that landslides occur in both urban and rural areas, using the SBAS technique can bring better results.

C- and X-band imagery acquired in the S1-A, and the CSK missions are satellite products that are particularly appropriate for retrieving deformation data of landslides under urban and rural areas because of their significant spatial resolution and short revisiting time of acquisition (Bovenga *et alii,* 2012; Fiaschi *et alii*, 2017).

In this study, S1-A, and CSK radar images were analyzed and compared for monitoring slow-moving landslide kinematics. Surface deformation and displacement time series were measured at CSK by applying the PSI technique and S1-A using the SBAS technique. In addition, the PSI and SBAS results were spatially georeferenced using a GNSS station in the stable area. An unsupervised machine learning algorithm (K-medians) (Ahuja

et alii, 2020) was used to prepare proper intervals to mean deformation rate maps (Khalili *et alii*, 2023). In addition, two additional GNSS stations located in the area affected by the deformation were compared with the outputs obtained from this study. The results of this study revealed that using different processing techniques (SBAS and PSI) and different SAR images in different bands can help us to investigate and analyze the kinematics of landslides more effectively and accurately.

CASE STUDY

The main campus of the University of Azuay is located in the city of Cuenca, south of Ecuador (South America), whose average height is 2,580 meters above sea level. This area has variable climatic conditions between dry periods (between June and November) and high levels of precipitation (between December and May), with an annual average of 940 mm (Sellers *et alii,* 2021).

The landslide of the University of Azuay is characterized as a complex landslide (rotational, translational and creeping movements) as a whole, the perforations carried out indicate various landslide sliding surfaces, the main ones being at a depth of 20 meters and a depth of 80 meters, making this landslide a Macroslide, with an approximate projected volume of more than 35 million cubic meters.

The geology of the study area is conformed mainly by the colluvial slope and alluvial deposits, the Turi and the Mangan formations. A large part of the southern highlands of Ecuador is covered by a layer of slightly consolidated and altered volcanic deposits. Pyroclasts predominate in sequence, consisting of agglomerates ranging from rhyolitic to andesitic, tuffs, volcanic ash, and ignimbrites, most of which are heavily kaolinized and/or silicified. The Turi formation comprises a well-stratified sequence of conglomerates and fluvial sands, clays, tuffs, and volcanic breccias, developed around the Cuenca basin and in broad areas of southern Ecuador. It is over 1200 meters thick and lies concordantly on the Ayancay (Santa Rosa) group, but also in certain places on the Macuchi and Yunguilla formations, a Pleistocene age is attributed to this formation (Steinmann, 1997) (Fig. 1).

The Mangan Formation conformed of three units. The lower unit includes the strata below the Washington lower coal seam. It consists predominantly of limonites, shales, and sandstones of fine grain and light colors, interspersed in layers less than 1 m thick. The middle unit comprises the strata from Washington's vein to the Cañari coal seam. And finally, above the Cañari coal seam, the upper unit consists mainly of coarse tuffaceous sandstones, with frequent pebbles, becoming increasingly conglomeratic upwards. Activity attributed to contemporary volcanic sedimentation is accentuated by the presence of various interbedded tuffs (Noblet *et alii*, 1988). A maximum thickness of 1,000 to 1,200 m is preserved in the west-central part of the basin (Steinmann, 1997). This formation is in the Upper Miocene to Pliocene ages (Hall & Calle, 1982; Sheppard, 1934; Steinmann, 1997). Colluvial slope deposits background relief of inter-Andean basins with partial pyroclastic cover, characterized by a heterogeneous mixture of fine materials and angular rock fragments, with the absence of stratification and internal ordering structures. Alluvial deposits are characterized by a mixture of sands, silts, clays, and conglomerates, representing the most significant proportion of the Cuenca basin.

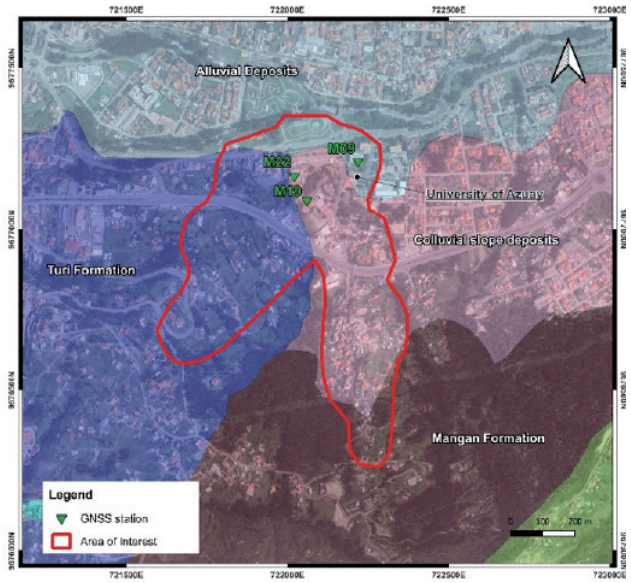

Fig. 1 - Geological sketch map of the case study (central sector of Cuenca), showing the basement complex, sedimentary basins, the study location (University of Azuay), and the location of three GNSS stations

Based on geological settings, the campus is classified as an unstable area due to the presence of materials such as clay and sandstone and a large amount of surface and underground water. It is in an area with soil saturation levels above eight meters according to the geophysical studies (Seismic Refraction & Reflection, drilling with core recovery) carried out in the area. These factors have triggered for many years (first evidences of this phenomena are recorded 1997) soil displacements that affect specific structures such as buildings, highway facilities, and civil works on the campus.

DATA SETS

In this study, C- and X-band imagery acquired from the S1-A, and CSK missions were used. These satellite products offer the advantage of significant spatial resolution and a short revisiting time, making them particularly suitable for deriving deformation data from our case study landslides in urban and rural areas.

S1-A is parts of the Copernicus program conducted by the European Commission in collaboration with the European Space Agency (ESA). The mission period is 12 days, and data analyses are achievable every six days; it also is an imaging Synthetic Aperture Radar mission operating in the C-band. In this study, the S1-A radar

images acquired between January 10, 2015, and November 26, 2018 (i.e., number of 61 SLC images) has been used respectively. Tab. 1 summarizes the characteristics of these acquired images.

In addition, CSK was commissioned and funded by the Italian Space Agency (ASI) and the Italian Ministry of Défense (MoD). A constellation of four medium-sized low-Earth orbit satellites is deployed, each equipped with a high-resolution multi-mode SAR sensor operating in the X-band. Depending on the availability of all four satellites (i.e., CSKS1, …, CSKS4), the CSK constellation can be revisited in up to four days. CSK launched its first satellite in June 2007, and the whole system has been operational since 2011. Fifty-five images were acquired over an ascending geometry track between March 12, 2016, and January 13, 2018, with a 40 x 40 km footprint have been used in this study. An overview of the acquired images can be found in Tab. 1. ERA5 reanalysis data published by the European Centre for Medium-Range Weather Forecasts are used to eliminate atmospheric, particularly tropospheric delays. This model published values of meteorological data, including water vapor pressure and temperature for 37 pressure levels. This study uses the same strategy to evaluate the obtained results from different SAR processing techniques on double-band SAR images (i.e., processing setting). Finally, this method uses the calculated displacements from observations of two GNSS stations in the study area.

	Mission	
	S1-A	CSK
Acquisition Time	January 10, 2015, November 26, 2018	March 12, 2016, and January 13, 2018
Type	SLC	SLC
Images (Nr)	61	57
Swath	IW2	-
Pass	Ascending	Ascending
Central Look Angle (°)	38	32
Polarization	VV	HH

Tab. 1 - Specifications of the Sentinel-1 and COSMO-SkyMed acquisitions.

METHODOLOGY

SAR Data Processing

A differential interferometry satellite aperture radar (Hanssen, 2001) has been demonstrated to be a helpful tool for measuring ground motions resulting from subsidence, landslides, earthquakes, and volcanic phenomena and monitoring structures and infrastructures. However, the DInSAR method is affected by spatial and temporal decorrelation, signal delays due to atmospheric effects, and orbital or topographic errors. Over time, the development of these techniques has allowed us to overcome some of the inherent limitations of the algorithms (temporal and spatial decorrelation, atmospheric disturbances, as mentioned above). Two primary approaches to interferometry are PSI (Hooper, 2008; Hooper *et alii*, 2004) and SBAS (Lanari *et alii*, 2004). By using these advanced DInSAR (A-DInSAR) techniques, the precision of the rate maps and time series of deformations has improved to about 1–2 mm/year and 5–10 mm, respectively.

PSI

By utilizing the PSI technique, radar targets (known as permanent scatters or PSs) (Crosetto *et alii*, 2016) are virtually immune from geometric and temporal interferometric effects and demonstrate high interferometric coherence because of their remarkably high stability over time. The Digital Elevation Model (DEM) used to implement this technique was chosen with a cell resolution of 3 m × 3 m, and a multi-looking factor was considered 3 × 3 in rage and azimuth, respectively. To apply the PSI method, the Coherent Pixels Technique (Mora *et alii*, 2003) implemented in SUBSIDENCE software, developed at Universitat Politecnica de Catalunya (UPC – Barcelona), has been used. This software processed the co-registered images, and all possible interferogram pairs (235) with spatial baselines lower than 300 meters were identified. A Temporal Phase Coherence threshold equal to 0.7 was set to select the points for further analyses. Finally, the line of sight (LoS) of the displacement rate map and time series were elaborated. It is noticed that this technique is implemented on CSK images.

SBAS

The SBAS method in the ISCE package was implemented using several steps, starting with data pre-processing, and ending with generating displacement maps and time series. The first step was the co-registration of the S1-A images using the precise orbit files provided by the ESA. After co-registration, the images were resampled to a typical grid to enable interferometric processing. The next step was interferogram generation, where all possible pairs of images were used to create interferograms. In the SBAS approach, only a subset of these interferograms was selected based on the baseline values to minimize temporal decorrelation effects. The resulting interferograms were then filtered to remove residual noise and atmospheric disturbances. After filtering, the differential interferograms were unwrapped to obtain the phase information, which was then converted to LoS displacement values. The unwrapped phase values for each pixel were analyzed over time to obtain the displacement time series. Finally, the displacement values were geocoded to generate displacement maps.

In the SBAS method (Berardino *et alii*, 2002), for S1-A images, the minimum threshold of Snaphu is considered 0.05,

the geocode threshold is considered 0.05, the spatial baseline orthogonal to the line-of-sight is 100 (m), and the temporal baseline is 90 (day). The DEM used to implement this technique was chosen with a cell resolution of 10 m × 10 m. Also, multi-looking was considered 3 × 9 for this technique in the ISCE package, co-registered images were processed, and all possible interferogram pairs (234). Finally, the LoS mean displacements rate map and time series of displacement were elaborated. It is noticed that this technique is implemented on S1-A images.

K-medians Unsupervised Clustering Algorithm

Clustering algorithms such as K-medians (Assent, 2012; Saleem, 2021) are used to cluster data. Clustering algorithms are designed to assign instances within a dataset to clusters based on their similarity rather than to instances belonging to other clusters. Three primary and variable features are used in this study: longitudes, latitudes, and velocities obtained from each processing method (PSI and SBAS) (Khalili et alii, 2023). In unsupervised clustering, five clusters are introduced to the algorithm, and a centroid is selected for each cluster based on the dataset available. Five clusters were selected based on knowledge from the study area to implement this algorithm. Each clustering algorithm's point or row is entered individually and measured with a different distance. After five updates, they will be placed in a proper cluster. Then we use the union–intersection principle, which is proportional to the clusters. An appropriate interval is determined by the number of points and their changes. Based on these algorithms' interval outputs, QGIS software produces mean deformation maps that are more accurate and reliable.

Evaluation by GNSS Stations

A time series of the relative positions of the receivers was derived using the Differential GPS (DGPS) technique, which involves utilizing two or more GNSS receivers to measure the difference in position between them. By comparing the raw observations from each receiver and applying differential corrections for atmospheric effects and other errors, it is possible to derive a time series of the receivers over time for evaluating our results obtained by different MT-InSAR techniques.

A comparison will be made between the results obtained from the above methodology and the GNSS dataset. The locations of the GNSS stations available in our case study area are shown in Fig. 1 (stations with time series available). It is noticed that to compare InSAR-derive results with GNSS data, both datasets must have the same datum (reference point).

When comparing InSAR-derived results with GNSS data, it is essential to ensure that both datasets are referenced to the same geodetic datum (i.e., the same reference point). This is because both InSAR and GNSS measurements are sensitive to the Earth's surface deformation, and the deformation can be expressed in different reference frames depending on the chosen datum. In this case, we have three GNSS stations, and the M09 station was located in the stable area. Therefore, we geo-referenced CSK and S1-A according to this station separately.

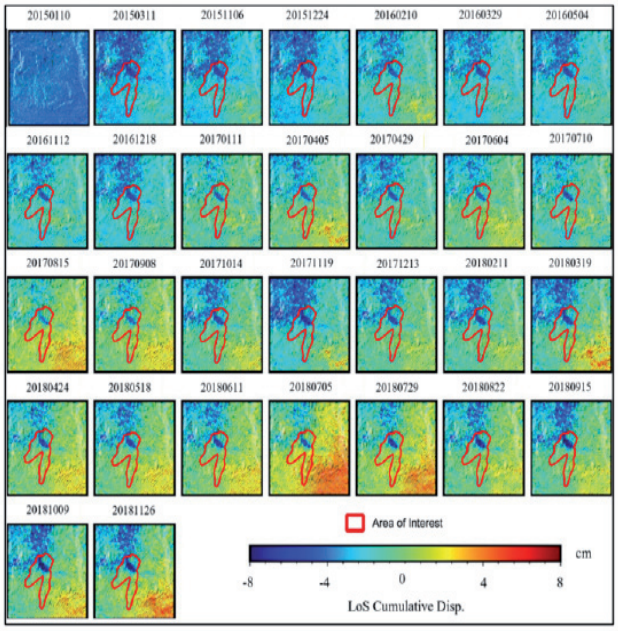

Fig. 2 - The time-series cumulative deformation maps along the LOS according to the SBAS technique (S1-A)

So, our InSAR and GNSS datasets have been compared using the same reference point, its location highlighted in Fig. 1.

RESULT AND DISCUSSION

Time Series of S1-A Cumulative Displacement

Based on S1-A images processed by the SBAS technique in the ISCE package, 61 time series cumulative displacement graphs of the University of Azuay landslide are obtained. It should be noted that all accumulated displacement was referenced in the first image, which was for S1-A on January 10, 2015, date (Fig. 2).

As can be seen in Figure 2, relating to the results of S1-A image processing, a significant shift (8 cm) can be observed in the central sector of the area, at the site where Azuay University is located, as early as March 2015. Further acceleration appears to have occurred in October 2017 and finally in July 2018 until the end of processing (November 2018). It is important to note that the negative values confirm the NW-SE direction of displacement and the direction of the deep slope of the area.

More precisely, the deformations in the southern part to the eastern and north-eastern parts are mainly positive in the LoS and reach up to nearly 6 cm from the eastern part to the south-eastern part. This analysis is critical for Azuay University and the deformations around it, which began on November 19, 2017, and continued until 6 cm of deformation along the LoS. Based on the analysis of S1-A

images, the eastern part of the region had positive deformation.

In contrast, the western part to north and north-western had negative deformation in the LoS direction, starting on February 10, 2016. The deformations then moved from the south to the north of the region as the landslide deformation behavior was changed and expanded to the middle and north parts of the area. In November 2016, the University of Azuay began to deform negatively, reached its maximum deformation of nearly 8 cm on February 11, 2018, and continued until September 15, 2018.

The deformation of the university of Azuay landslide exhibits evident spatial heterogeneity, with the most considerable deformation in the middle to the east and south part of the landslide, followed by the landslide toe and deformation at the landslide crown.

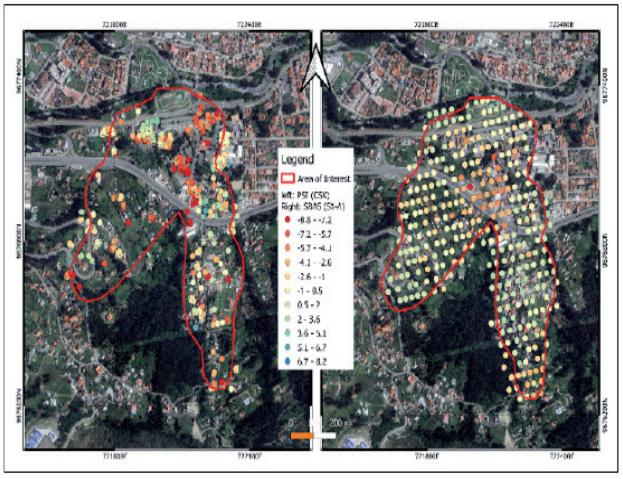

Fig. 3 - The mean deformation rate maps along the LOS according to left) PSI (CSK), and right) SBAS (S1-A)

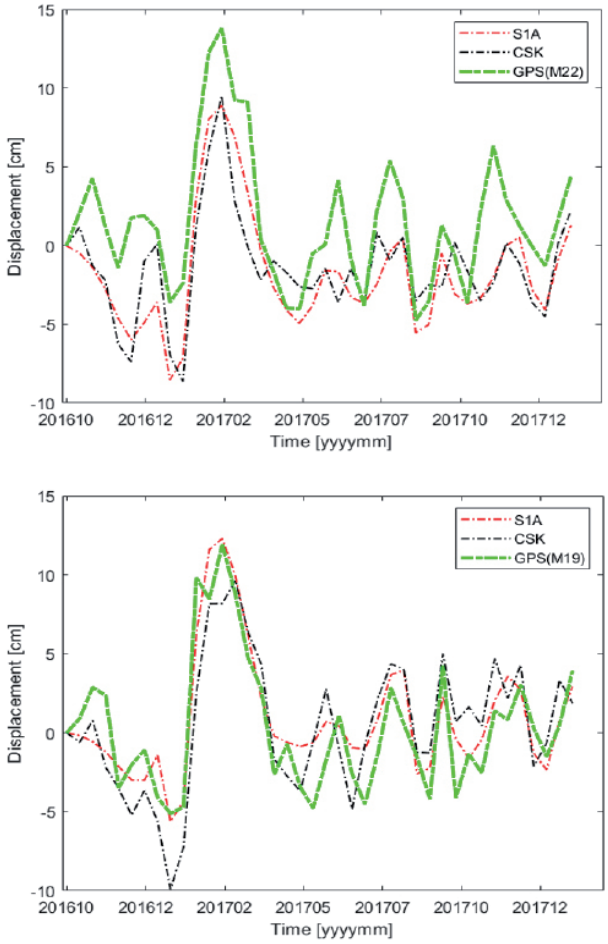

Fig. 4 - Comparison of GNSS and InSAR time-series derived from Sentinel-1A and COSMO-SkyMed data at GNSSstation M22

Mean Deformation Rate Map

Before investigating and analyzing the deformation rate obtained from each technique and different SAR images, it is necessary to highlight that the K-medians were used to determine the precision, reliability, and best interval for monitoring straightforward mean deformation rate map and finding the zones of risk to better decipher displacement distribution patterns for better understanding and interpretation. The mean deformation rate map (Fig. 3) has been created using the output intervals from the K-medians clustering algorithm.

In this study, the SBAS and PSI techniques are utilized to analyze the mean deformation rate of the University of Azuay landslide in the radar LOS direction applied to S1-A and CSK, respectively. As shown in Figure 3, the mean deformation rate of the University of Azuay landslide in the LoS direction ranges from −1 to -9 cm/year, and the mean velocity along LoS ranges from −9 to +7 cm/year in the central to the east sector of the study area in both CSK and S1-A images. Additionally, since the PSI method failed to detect PSs in the CSK images related to the highway section, which did not display deformations, the SBAS technique was able to cover the remaining deformation effects resulting from the landslide, which ranged from -8 to -1 cm/year, due to the presence of DSs in the processed S1-A images.

In the processing of CSK images between March 12, 2016, and January 13, 2018, most of the deformation was related to the central part of the case study from -9 to -2 cm/year, while S1-A images were processed to illustrate the complete landslides from January 10, 2015, November 26, 2018, and October 01, 2016, and November 20, 2018, with ranges from -7 to -1 cm/year which was shown in cumulative deformation how the landslides of this study area were completed that both the deformation in Azuay University and the highway near the centre of the study area were covered. The upper and lower sectors did not display significant movements, except for the most up-sector of the southern slope, where values lower than -2 cm/year were observed, and deformation did not change significantly. The landslide deformation is concentrated in the middle with a longitudinal length of approximately 600-700 m.

Evaluation by GNSS Stations

GNSS 3D displacement measurements are projected to the same reference date along the LoS as the InSAR time series to compare results. To comparison was initially performed for the two GNSS time series between the 2016- and 2018-time span. Also, to match GNSS and InSAR time series to one common period, we used spline interpolation. Results illustrate that the GNSS time series are in good agreement with the InSAR time series (Fig. 4). In this analysis, this comparison ensures that the cumulated displacement is valid and effective for the investigation of displacement caused by landslides. To express the results more precisely, it can be said that the cumulative displacements obtained from the SBAS technique with the C-band images are more similar in behavior to the cumulative displacements obtained from the two GNSS stations. Furthermore, even though the total period in the GNSS stations is close to zero displacements, the accuracy of the work done with both techniques and both types of SAR images confirm periodic deformation behaviours which is due to seasonal rainfall in the months of November to February.

CONCLUSION

The results obtained from this study reveal that: depending on the geological setting of the study area, there is a significant displacement rate, and several movements occur in the northern and north-eastern parts of the landslide area as well as in the urban areas. As it was obtained from the techniques and images in different bands, this displacement rate reached its highest value, mainly at Azuay University and the highway near the university. Another sector of the landslide occurs in rural areas in the central part. In other parts, which are supposed to justify the shape of the landslide, they are smooth and without deformation.

The CSK images processed with the PSI technique did not capture the complete deformations and patterns of the landslide, as discussed in the previous section. However, our landslides at Azuay University and along the highway were analyzed with C-band images (S1-A) processed with the SBAS technique. Additionally, comparing the results with two GNSS stations confirmed the excellent agreement between radar image processing and GNSS results. We could accomplish better alignment and accuracy with S1-A than with the proximity of GNSS and DS points, and the cumulative deformation justified the decision.

Based on the analyses and the geological data collected in the study area, most deformations were found in the colluvial slopes and alluvial deposits. Different techniques and double-band SAR images confirmed that the types of formations in the case study could be an essential parameter in investigating Cuenca's landslides.

Finally, for better handling the issue of displacements based on landslides and having enough information for review and analysis, especially since we are in an area containing both urban and rural types, it is necessary to use images with different bands and process them with different techniques to get accurate landslide kinematics results.

REFERENCES

Ahuja R., Chug A., Gupta S., Ahuja P. & Kohli S. (2020) - *Classification and clustering algorithms of machine learning with their applications.* Nature-inspired computation in data mining and machine learning, **855**: 225–248. https://doi.org/10.1007/978-3-030-28553-1_11

Ajmera b. & Tiwari b. (2021) - *Recent advances in the methods of slope stability and deformation analyses.* In Tiwari K. Sassa P., T. Bobrowsky T. & Takara K. (eds.), *Understanding and reducing landslide disaster risk.* Testing, modeling and risk assessment, volume **4**: 81–108. Springer international publishing. https://doi.Org/10.1007/978-3-030-60706-7_5

Allocca V., Di Napoli M., Coda S., Carotenuto F., Calcaterra D., Di Martire D. & De Vita P. (2021) - *A novel methodology for Groundwater Flooding Susceptibility assessment through Machine Learning techniques in a mixed-land use aquifer.* Science of the total environment, **790**: 48067.

Assent I. (2012) - *Clustering high dimensional data.* WIREs Data Mining and Knowledge Discovery, **2**(4): 340–350. https://doi.org/10.1002/widm.1062

Atanasova-Zlatareva M. & Nikolov H. (2017) - *Displacements Monitoring of The Trifon Zarezan Landslide by Gnss Observations And Insar Introduction.* 2017(**1**): 1–5. https://doi.org/10.3997/2214-4609.201702567

Berardino P., Fornaro G., Lanari R. & Sansosti E. (2002) - *A new algorithm for surface deformation monitoring based on small baseline differential SAR interferograms.* IEEE Transactions on Geoscience and Remote Sensing, **40**(11): 2375–2383. https://doi.org/10.1109/TGRS.2002.803792

Bovenga F., Wasowski J., Nitti D. O., Nutricato R. & Chiaradia M. T. (2012) - *Using COSMO/SkyMed X-band and ENVISAT C-band SAR interferometry for landslides analysis.* Remote Sensing of Environment, **119**: 272–285. https://doi.org/10.1016/j.rse.2011.12.013

Coda S., Confuorto P., De Vita P., Di Martire D. & Allocca V. (2019) - *Uplift Evidence Related to the Recession of Groundwater Abstraction in a Pyroclastic-Alluvial Aquifer of Southern Italy.* Geosciences, **9**(5), Article 5. https://doi.org/10.3390/geosciences9050215

Coda S., Tessitore S., Di Martire D., Calcaterra D., De Vita P., & Allocca V. (2019) - *Coupled ground uplift and groundwater rebound in the metropolitan city of Naples (southern Italy).* Journal of Hydrology, **569**: 470–482. https://doi.org/10.1016/j.jhydrol.2018.11.074

Crosetto M., Monserrat O., Cuevas-González M., Devanthéry N. & Crippa B. (2016) - *Persistent Scatterer Interferometry: A review. ISPRS* Journal of Photogrammetry and Remote Sensing, **115**: 78–89. https://doi.org/10.1016/j.isprsjprs.2015.10.011

Del Soldato M., Confuorto P., Bianchini S., Sbarra P. & Casagli N. (2021) - *Review of works combining GNSS and InSAR in Europe.* Remote Sensing, **13**(9):1684.

Ferretti A., Prati C. & Rocca F. (2001) - *Permanent scatterers in SAR interferometry.* IEEE Transactions on Geoscience and Remote Sensing, **39**(1): 8–20. https://doi.org/10.1109/36.898661

Fiaschi S., Tessitore S., Bonì R., Di Martire D., Achilli V., Borgstrom S., Ibrahim A., Floris M., Meisina C., Ramondini M. & Calcaterra D. (2017) - *From ERS-1/2 to Sentinel-1: Two decades of subsidence monitored through A-DInSAR techniques in the Ravenna area (Italy).* GIScience & Remote Sensing, **54**(3): 305–328. https://doi.org/10.1080/15481603.2016.1269404

Foumelis M., Papageorgiou E. & Stamatopoulos C. (2016) - *Episodic ground deformation signals in Thessaly Plain (Greece) revealed by data mining of SAR interferometry time series.* International Journal of Remote Sensing, **37**(16): 3696–3711. https://doi.org/10.1080/01431161.2016.1201233

Gabriel A. K., Goldstein R. M. & Zebker H. A. (1989) - *Mapping small elevation changes over large areas: Differential radar interferometry.* Journal Of Geophysical Research: Solid Earth, **94**(B7): 9183–9191. https://Doi.Org/10.1029/Jb094ib07p09183

Ghorbanzadeh O., Xu Y., Zhao H., Wang J., Zhong Y., Zhao D., Zang Q., Wang S., Zhang F., Shi Y., Zhu X. X., Bai L., Li W., Peng W. & Ghamisi P. (2022) -*The Outcome of the 2022 Landslide4Sense Competition: Advanced Landslide Detection from Multisource Satellite Imagery.* IEEE Journal of Selected Topics in Applied Earth Observations and Remote Sensing, **15**: 9927–9942. https://doi.org/10.1109/JStars.2022.3220845

Guerriero L., Confuorto P., Calcaterra D., Guadagno F. M., Revellino P. & Di Martire D. (2019) - *PS-driven inventory of town-damaging landslides in the Benevento, Avellino and Salerno Provinces, southern Italy.* Journal of Maps, **15**(2): 619–625. https://doi.org/10.1080/17445647.2019.1651770

Hall M. L. & Calle J. (1982) - *Geochronological control for the main tectonic-magmatic events of Ecuador.* Earth-Science Reviews, **18**(3): 215–239. https://doi.org/10.1016/0012-8252(82)90038-1

Hanssen R. F. (2001) - *Radar Interferometry: Data Interpretation and Error Analysis.* Springer Science & Business Media.

Hooper A. (2008) - *A multi-temporal InSAR method incorporating both persistent scatterer and small baseline approaches.* Geophysical Research Letters, **35**(16). https://doi.org/10.1029/2008GL034654

Hooper A., Zebker H., Segall P. & Kampes B. (2004) - *A new method for measuring deformation on volcanoes and other natural terrains using InSAR persistent scatterers.* Geophysical Research Letters, **31**(23). https://doi.org/10.1029/2004GL021737

Khalili M. A., Voosoghi B., Guerriero L., Haji-Aghajany S., Calcaterra D. & Di Martire D. (2023) - *Mapping of Mean Deformation Rates Based on APS-Corrected InSAR Data Using Unsupervised Clustering Algorithms.* Remote Sensing, **15**(2): Article 2. https://doi.org/10.3390/rs15020529

Lanari R., Mora O., Manunta M., Mallorqui J. J., Berardino P. & Sansosti E. (2004) - *A small-baseline approach for investigating deformations on full-resolution differential SAR interferograms.* IEEE Transactions on Geoscience and Remote Sensing, **42**(7): 1377–1386. https://doi.org/10.1109/TGRS.2004.828196

Lu Y., Liu G., Cui K. & Zheng J. (2021) - *Mechanism and Stability Analysis of Deformation Failure of a Slope.* Advances in Civil Engineering, Volume 2021, Article ID 8949846: 16 pp. https://doi.org/10.1155/2021/8949846

Miele P., Di Napoli M., Guerriero L., Ramondini M., Sellers C., Annibali Corona M. & Di Martire D. (2021) - *Landslide Awareness System (LAwS) to increase the resilience and safety of transport infrastructure: the case study of Pan-American Highway (Cuenca–Ecuador).* Remote Sensing, **13**(8): Article 8. https://doi.org/10.3390/rs13081564

Mora O., Mallorqui J. J. & Broquetas A. (2003) - *Linear and nonlinear terrain deformation maps from a reduced set of interferometric SAR images*. In IEEE Transactions on Geoscience and Remote Sensing, **41**(10) : 2243-2253. Doi: 10.1109/TGRS.2003.814657.

Noblet C., Lavenu A. & Schneider F. (1988) - *Etude géodynamique d'un bassin intramontagneux tertiaire sur décrochements dans les Andes du Sud de l'Equateur: L'exemple du bassin de Cuenca.* https://www.semanticscholar.org/paper/Etude-g%C3%A9odynamique-d'un-bassin-intramontagneux-sur-Noblet-Lavenu/70f785de5cc050b47f1a132aa6217b5c6210dc68

Petrucci O. (2022) - *Landslide Fatality Occurrence: A Systematic Review of Research Published between January 2010 and March 2022.* Sustainability, **14**(15): Article 15. https://doi.org/10.3390/su14159346

Saleem A. (2021) - *Remote Sensing by using Unsupervised Algorithm (No. 2021070257).* Preprints. https://doi.org/10.20944/preprints202107.0257.v1

Sellers C. A., Buján S. & Miranda D. (2021) - *MARLI: A mobile application for regional landslide inventories in Ecuador.* Landslides, **18**(12): 3963–3977. https://doi.org/10.1007/s10346-021-01764-9

Sheppard G. (1934) - *Geology of the Interandine Basin of Cuenca, Ecuador.* Geological Magazine, **71**(8): 356–370. https://doi.org/10.1017/S0016756800093596

Soltanieh A. & Macciotta R. (2022) - *Updated Understanding of the Thompson River Valley Landslides Kinematics Using Satellite InSAR.* Geosciences, **12**(10): Article 10. https://doi.org/10.3390/geosciences12100359

Steinmann M. (1997) - *The Cuenca Basin of Southern Ecuador: Tectono-sedimentary History and the Tertiary Andean Evolution.* A dissertation submitted to the Swiss Federal Institute of Technology Zurich for the degree of Doctor of natural sciences. Swiss Federal Institute of Technology Zurich.

Wasowski J. & Bovenga F. (2014) - *Investigating landslides and unstable slopes with satellite Multi Temporal Interferometry: Current issues and future perspectives.* Engineering Geology, **174**: 103-138.

Received February 2023 - Accepted March 2023